Laboratory Investigation (2021) 101:204–217
https://doi.org/10.1038/s41374-020-00494-1

ARTICLE

Establishing a living biobank of patient-derived organoids of intraductal papillary mucinous neoplasms of the pancreas

Francisca Beato[1] · Dayana Reverón[2] · Kaleena B. Dezsi[3] · Antonio Ortiz[4] · Joseph O. Johnson[4] · Dung-Tsa Chen[5] · Karla Ali[3] · Sean J. Yoder[6] · Daniel Jeong[7] · Mokenge Malafa[1] · Pamela Hodul[1] · Kun Jiang[8] · Barbara A. Centeno[8] · Mahmoud A. Abdalah[9] · Jodi A. Balasi[10] · Alexandra F. Tassielli[1] · Bhaswati Sarcar[1] · Jamie K. Teer[5] · Gina M. DeNicola[11] · Jennifer B. Permuth[1,3] · Jason B. Fleming[1]

Received: 17 December 2019 / Revised: 17 September 2020 / Accepted: 17 September 2020 / Published online: 9 October 2020

Abstract

Pancreatic cancer (PaCa) is the third leading cause of cancer-related deaths in the United States. There is an unmet need to develop strategies to detect PaCa at an early, operable stage and prevent its progression. Intraductal papillary mucinous neoplasms (IPMNs) are cystic PaCa precursors that comprise nearly 50% of pancreatic cysts detected incidentally via cross-sectional imaging. Since IPMNs can progress from low- and moderate-grade dysplasia to high-grade dysplasia and invasion, the study of these lesions offers a prime opportunity to develop early detection and prevention strategies. Organoids are an ideal preclinical platform to study IPMNs, and the objective of the current investigation was to establish a living biobank of patient-derived organoids (PDO) from IPMNs. IPMN tumors and adjacent normal pancreatic tissues were successfully harvested from 15 patients with IPMNs undergoing pancreatic surgical resection at Moffitt Cancer Center & Research Institute (Tampa, FL) between May of 2017 and March of 2019. Organoid cultures were also generated from cryopreserved tissues. Organoid count and size were determined over time by both Image-Pro Premier 3D Version 9.1 digital platform and Matlab application of a Circular Hough Transform algorithm, and histologic and genomic characterization of a subset of the organoids was performed using immunohistochemistry and targeted sequencing, respectively. The success rates for organoid generation from IPMN tumor and adjacent normal pancreatic tissues were 81% and 87%, respectively. IPMN organoids derived from different epithelial subtypes showed different morphologies in vitro, and organoids recapitulated histologic and genomic characteristics of the parental IPMN tumor. In summary, this preclinical model has the potential to provide new opportunities to unveil mechanisms of IPMN progression to invasion and to shed insight into novel biomarkers for early detection and targets for chemoprevention.

Introduction

Pancreatic cancer (PaCa) poses a significant mortality burden globally. It is currently the seventh leading cause of cancer-related deaths worldwide [1] and the third leading cause in the United States (US) [2]. Approximately 57,600 patients will be diagnosed with pancreatic cancer this year in the US and an estimated 47,050 patients will die from this malignancy [3]. Despite advances in its diagnosis and treatment, it holds the lowest 5-year relative survival rate of all leading cancers, at 9–10% [3]. PaCa incidence and mortality rates are increasing [4–8], and it is predicted to become the second leading cause of cancer mortality around 2020, surpassing colorectal, prostate, and breast cancers [9]. There is an unmet need to develop strategies to detect PaCa at an early, operable stage and prevent its progression.

Intraductal papillary mucinous neoplasms (IPMNs) are cystic PaCa precursors that comprise nearly 50% of pancreatic cysts detected incidentally via computed tomography (CT) scans and magnetic resonance imaging [10, 11].

These authors contributed equally: Francisca Beato, Dayana Reverón

These authors jointly supervised this work: Jennifer B. Permuth, Jason B. Fleming

Supplementary information The online version of this article (https://doi.org/10.1038/s41374-020-00494-1) contains supplementary material, which is available to authorized users.

✉ Jason B. Fleming
Jason.fleming@moffitt.org

Extended author information available on the last page of the article

Unfortunately, once detected, noninvasive strategies to accurately distinguish benign IPMNs that can undergo surveillance from malignant IPMNs that warrant surgical resection are lacking, posing a clinical conundrum. IPMNs can present in the main pancreatic duct (MD-IPMN), side branch ducts (BD-IPMN), or both (mixed-IPMN). Based on cytoarchitectural features and mucin protein profiles assessed pathologically after tissue has been resected, IPMNs are classified into four histopathological types: gastric, intestinal, pancreatobiliary, and oncocytic, with the pancreatobiliary subtype having the poorest prognosis [12, 13].

Up to 70% of resected MD-IPMNs harbor high-grade dysplasia or invasive disease [14, 15] and have a risk of recurrence up to 65% if invasive disease is present [16]. Of patients diagnosed with well- and poorly-differentiated unresectable IPMNs, clinical surveillance studies show malignant progression within 10 years in up to 8% and 25% of cases, respectively [15–17]. Taken together, because IPMNs can progress to invasive, fatal malignancy, the study of these lesions offers a prime opportunity to develop early detection and prevention strategies.

The organoid culture approach provides a potential framework for preclinical and clinical PaCa research focused on early detection and prevention. This resourceful three-dimensional (3D) culture model recapitulates the structural features, mutational spectrum, tumor heterogeneity and therapeutic sensitivity profiles of primary pancreatic tumors [18–21]. Although patient-derived organoid (PDO) models exist for microscopic pancreatic cancer precursors known as pancreatic intraepithelial neoplasms [22], our team sought to develop one of the first sets of IPMN PDO models paired with normal tissue. While we were in the process of resubmitting this manuscript, another team [23] reported on a living IPMN biobank where they generated organoids from seven normal pancreatic ducts and ten unpaired IPMN tumor samples.and performed molecular characterization. The aims of the current study were to: (1) establish a human organoid model of paired premalignant and normal tissue cultures from resected IPMN specimens; (2) demonstrate the passage and cryopreservation of organoid cultures as part of a living biobank infrastructure; (3) generate preinvasive organoid cultures from cryopreserved resected pancreatic tissue; (4) establish a reliable protocol for imaging and counting of the organoids via a digital platform; and (5) characterize the primary tumors and organoid cultures by genomic analysis.

Materials and methods

Patient recruitment and tissue collection

Patients diagnosed with resectable pancreatic lesions between May of 2017 and March of 2019 at the Moffitt Cancer Center & Research Institute (Tampa, Florida) were recruited to participate in two complementary Institutional Review Board-approved studies known as the Total Cancer Care Protocol and the Florida Pancreas Collaborative study [24]. None of these cases received treatment with chemotherapy or radiation prior to surgery. Tumor and adjacent normal pancreatic tissues were obtained from the surgical suite, harvested, and reviewed by a pancreatic pathologist (BAC or KJ), to verify the diagnosis and to identify tumor and adjacent normal nonneoplastic pancreas tissue. By histology and immunohistochemistry techniques, the epithelial subtype of the IPMN was determined [12, 13]. Both collection and transport of the tissue samples were facilitated by the Moffitt Tissue Core Acquisition Team. The laboratory specialist received the pair of tumor and normal samples within ~20 min of the operative procedure in order to establish tumor and normal organoid cultures as described below. The workflow from tissue collection to organoid culture characterization is shown in Fig. 1.

Organoid culture media

Wash Media consisted of Advanced DMEM/F12 medium supplemented with HEPES [1×, Invitrogen], Glutamine [1×, VWR] or Glutamax [1×, Invitrogen] and Primocin [1×, 50 mg/mL, InvivoGen].

Digestion Media consisted of wash media supplemented with collagenase type IV from Clostridium histolyticum [5 mg/mL, Gibco] and Dispase [1 mg/mL, Sigma].

Complete Growth Media consisted of 50% wash media without FBS, 50% conditioned media [Wnt3a/R-Spondin/Noggin, L-WRN ATCC] supplemented with B27 [1×, Invitrogen], Nicotinamide [10 mM], N-acetyl-L-cysteine [1.25 mM, Sigma], Primocin [100 µg/mL], mNoggin [100 ng/mL], human epidermal growth factor [hEGF, 50 ng/mL, Peprotech], human fibroblast growth factor 10 [100 ng/mL, Peprotech], Gastrin [10 nM, Sigma], A 83-01 [500 nM, Tocris], PGE2 [1 µM, R&D Systems], and Y-27632 [10.5 µM, Sigma].

Cell Recovery Solution (Corning), Recovery Cell culture Freezing Medium (Thermo Fisher).

Generation and expansion of patient-derived organoids from fresh resected specimens

IPMN tumor and normal pancreatic organoids were generated and expanded by modification of previously-described protocols of PaCa organoids [22, 25–27]. Following resection and receipt of tissues by the lab specialist, tissue samples were placed into separate 50 mL Falcon tubes containing wash media then transferred to a 10 cm dish. A tissue size of 0.25–4 cm^2 was ideal to move forward with processing. Both tissue types were minced into 1 mm^3 fragments. Fragments were transferred to a 15 mL tube into

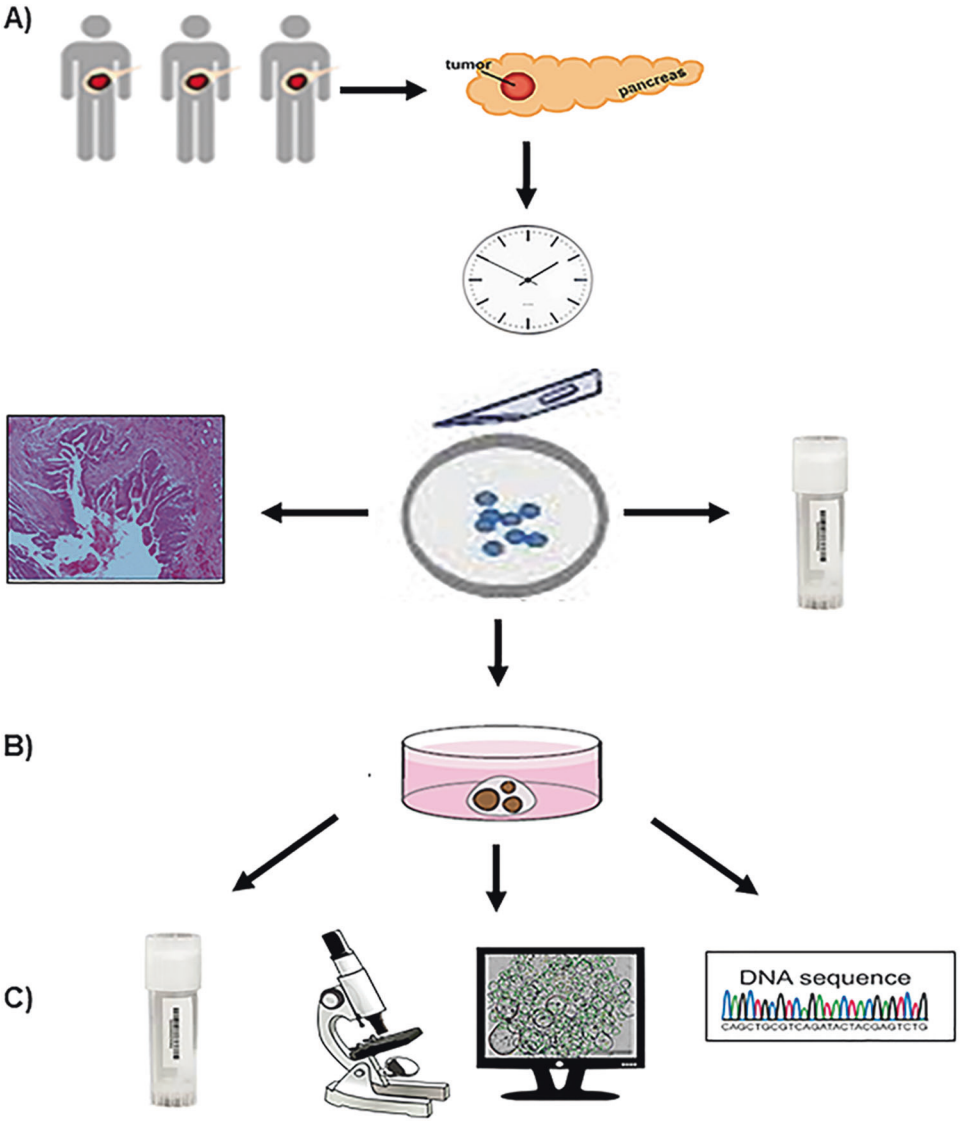

Fig. 1 Workflow of patient-derived IPMN organoid culture methodology. **a** Resected IPMN tumor and adjacent normal tissues obtained from patients were transported to the processing lab within 20 min of resection; and a portion of each type of tissue was cryopreserved. Primary tissue was analyzed by histomorphology and immunohistochemistry analysis. Both IPMN tumor and adjacent normal tissue specimens were minced into small pieces and subsequently subjected to organoid culture. **b** 3D-organoid cultures from both tumor and normal tissues were established. **c** Organoids were cryopreserved and culture was imaged via bright-field microscopy, automated counting was conducted via the Circular Hough Transform-based algorithm, and characterized by genomic DNA fingerprinting and sequencing.

which 6 mL of modified digestion media was added. The tube was incubated for 30–45 min in a 37 °C shaker with agitation at 500 rpm to allow tissue to dissociate into single cells. Fragments were allowed to settle under normal gravity for 2 min and the supernatant was transferred to a clean Falcon tube. An additional 3 mL of wash media containing 10% FBS was added and the tube was centrifuged at 1300 rpm for 5 min The pellet was washed one more time as above. Cell pellets were then re-suspended in 300 µL of ice-cold growth factor reduced Matrigel. 50 µL domes were loaded onto six wells of a pre-warmed 24-well culture plate and allowed to solidify on an incubator for 15 min at 37 °C, 5% CO_2. Next, 500 µL of pre-warmed complete growth media was added per well and incubated at 37 °C, 5% CO_2. The growth and quantity of the organoid cultures were monitored for up to 14 days. Within that period, fresh growth media was added every 2 days.

At the conclusion of the 2-week-incubation, expansion of the organoid cultures was conducted by harvesting from one confluent well. To break apart the Matrigel, 1 mL of cold cell recovery solution or splitting media was added to the well and pipetted up and down. The suspension was incubated in a 15 mL Falcon tube on ice for 30 min, inverted every 10 min, and then centrifuged at 1300 rpm for 6 min at 4 °C. The pellet was re-suspended in wash media with 0.1% BSA and washed as above, then re-suspended in Matrigel and plated among 3–5 wells of a 24-well plate depending upon organoid size. For example, from a confluent well, smaller organoids (5–50 px.) would be plated into three wells, while larger organoids (50–200 px.) would be plated into five wells. The culture was allowed to solidify and incubated as described above. The organoid cultures were passaged up to four times.

Generation and expansion of patient-derived organoids from cryopreserved specimens

Organoids were also derived from cryopreserved specimens with the ultimate goal of determining the viability of premalignant organoids cultured from frozen specimens. To accomplish this, following resection, tissue was transferred to a cryovial preloaded with 1 mL of CryoStor CS10 freezing solution (Stem CT) and placed on ice for 30 min, then stored in a Mr. Frosty freezing container at −80 °C overnight prior to liquid nitrogen storage. Tissue was thawed in a 37 °C water bath until 50% thawed and transferred to a 100 mm petri dish containing wash media. Tissue was minced and digested as above.

Freezing and reviving of patient-derived organoids

Organoids from fresh and frozen tissue were harvested using cell recovery solution (1 mL per well), incubated on ice for 30 min, inverted every 10 min and spun at 1300 rpm for 6 min at 4 °C. The pellet was re-suspended in wash media with 1% BSA, washed as previously described, and then frozen in 500 µL of cell recovery freezing media. To revive the organoids, the frozen vial was placed in a 37 °C water bath until 50% was thawed. The vial was then rinsed with wash media containing 1% BSA and 0.1% Y-27632 Rho kinase inhibitor to help the cells cope with freeze/thaw stress. An additional 3 mL of media were added and the tube was centrifuged at 1300 rpm for 6 min The resulting pellet was re-suspended in cold Matrigel as previously described. In most cases, the organoids began appearing in culture by 3 days-post thaw.

Imaging and digital quantification of patient-derived organoids in vitro

Organoid culture images were acquired on a Zeiss Axio inverted Fluorescence Microscope system using the Zen 2.3 pro analysis and an EVOS FL Auto Imaging System with an Olympus PlanApo N 1.25×/0.04 objective. *Z*-stacks were obtained on the EVOS FL through the entire volume of the Matrigel in order to capture most of the organoids. Following image acquisition on the EVOS, images were preprocessed and flattened to reduce shadowing effect using Image-Pro Premier Version 9.1. In order to detect the overlapped circular objects, the images were first pre-processed to filter noise, enhance contrast, and enhance the edges. Then, using Matlab a Circular Hough Transform (CHT) based algorithm was used to find the overlapped circular objects in each image. Resulting counts were then plotted and analyzed with the assistance of the Moffitt Analytic Microscopy Core Facility.

Genomic characterization of patient-derived organoids

DNA isolation and quality control

DNA was isolated from both fresh and frozen organoid cultures utilizing the DNeasy Blood & Tissue Kit from Qiagen (Cat. No. 69504). Once DNA was isolated from the organoid cultures, the concentration, volume, and DNA integrity number (DIN). DIN score were determined using Qubit fluorometric quantitation and the Agilent TapeStation Genomic DNA ScreenTape Assay.

Preparation of fresh organoids for DNA isolation

To prepare the organoids from culture, the media from one to two confluent wells was aspirated. Cell recovery medium was added (1 mL per well) and pipetted up and down until the Matrigel broke down in solution. The mixture was transferred to a 2 mL tube and incubated on ice for 45–60 min The mixture was then centrifuged at 6000 RCF for 3 min at 4 °C and supernatant was removed followed by re-suspension in 200 µL ice-cold PBS with 0.1% BSA for an initial wash. The solution was triturated vigorously up to 20 times with a P200 pipette. PBS with 0.1% BSA (1 mL) was added to the solution and the tube was centrifuged at 6000 RCF for 3 min at 4 °C. The supernatant was removed and subsequent steps were repeated for a second wash. The Qiagen DNeasy Blood & Tissue Kit protocol was then followed for DNA isolation.

Preparation of frozen organoids for DNA isolation

To prepare the cryopreserved organoid cultures for DNA isolation, the cryopreserved vial was thawed in a 37 °C water bath for 1–2 min The cell suspension was placed in a 5 mL tube with 3 mL of cold human wash medium with 0.1% BSA and centrifuged at 400 RCF for 5 min at 4 °C. The supernatant was aspirated and the pellet was re-suspended in 200 µL ice-cold PBS with 0.1% BSA. The suspension was transferred to a 1.5 mL Eppendorf tube and triturated vigorously to blend organoids into solution. Ice-cold PBS with 0.1% BSA (1 mL) was added and the tube was centrifuged at 6000 RCF for 3 min at 4 °C. The resulting supernatant was discarded and the Qiagen DNeasy Blood & Tissue Kit protocol was then followed for DNA isolation.

DNA fingerprinting

To assess sample quality and integrity and establish sample identity, 34–42 ng (15 ng/µL) of isolated DNA from each sample was aliquoted and used to generate a DNA

fingerprint with the 96-SNP Advanta™ SampleID Genotyping Panel (Fluidigm, Inc). Briefly, the DNA samples were pre-amplified using the Advanta specific target amplification primers according to the manufacturer's protocol and the amplified DNA along with the Advanta SampleID allele-specific and locus-specific primers were transferred to a Fluidigm 96.96 Dynamic Array Integrated Fluidics Circuit (IFC) for Genotyping. The IFC was processed on the Fluidigm Juno IFC Controller, and real-time PCR was performed on the Fluidigm Biomark HD System and the data were reviewed in the Fluidigm Genotyping Analysis Software.

Histology and immunohistochemistry

To determine whether morphological features are preserved in the organoids, we performed hematoxylin and eosin (H&E) and immunohistochemical (IHC) staining for MUC5AC (mouse monoclonal antibody, Ventana, Inc), the cancer epithelial marker cytokeratin-19 (CK19) (mouse monoclonal antibody, Ventana, Inc), and Ki-67 (rabbit monoclonal antibody, Ventana, Inc) in both the organoids and their parental tumor tissue. Organoids were revived from frozen organoid culture or generated from fresh tissue. Briefly, 500 µL of Dispase (5 U/mL) diluted 1:5 in HBSS was added per well and incubated for 10 min at 37 °C, 5% CO_2 incubator. Organoid suspension from one confluent or two semi-confluent wells were harvested and transferred to a 1.5 mL Eppendorf tube and centrifuged at 1500 rpm for 6 min

The pellet was washed once with 1× PBS and resuspended in 1 mL of 4% PFA and incubated at room temperature for 30 min or overnight at 4 °C. The suspension was centrifuged as above and the pellet was washed twice with 1× PBS. To form a plug, the pellet was resuspended in 100 µL of warmed Histogel and allowed to polymerize at 4 °C for 10 min. The organoid plug was removed from the Eppendorf tube and transferred to a 5 mL tube containing 2 mL of 70% ethanol and sent to the histology lab. Organoids were paraffin embedded and subjected to serial sections for H&E and IHC following per standard histology lab operating procedures.

Targeted DNA sequencing

As proof-of-concept, we evaluated the genomic similarity between a set of four tumor organoids and their primary parental tumor and normal tissue by isolating DNA and conducting targeted sequencing of 275 cancer-related genes using the QIAseq Human Comprehensive Cancer Panel. Forty nanograms of DNA was fragmented and used to construct whole-genome DNA libraries, followed by a single-primer extension-based target enrichment and library final amplification according to the manufacturer's protocol. Following screening on the Agilent TapeStation 4200, the libraries were qPCR-quantitated using the Kapa Library Quantification Kit (Roche, Inc.), and the libraries were sequenced with a 2×150 base paired-end sequencing run on the Illumina NextSeq 500. After sequencing, the results were analyzed with the Qiagen QIAseq Targeted Sequencing Data Analysis Portal. Somatic mutations were determined by subtracting any variant observed in the normal sample from the passing variants detected in the parent IPMN or PDO samples. Identity was again confirmed by comparing genotypes at common polymorphisms.

Results

Tissue samples from 15 unique IPMN surgical cases were processed to harvest organoids from paired IPMN tumor and adjacent normal pancreatic tissues. The cases included nine male and six female patients ranging from 61 to 88 years of age at the time of resection, of which 40% were diagnosed due to incidental findings on CT imaging (Fig. 2a). The IPMN specimens were resected from varying locations in the pancreas including the pancreatic head, uncinate process, body, and tail. The IPMN cohort included three low-grade IPMNs, two moderate-grade IPMNs, seven high-grade IPMNs, and three IPMNs associated with invasive carcinoma. Several distinct epithelial subtypes were characterized by histology and immunohistochemistry including pancreatobiliary, intestinal, and mixed subtypes (Fig. 2b). Further details regarding select clinicopathological characteristics of the IPMN study cohort are listed in Table 1.

Generation of IPMN organoid models

Among the 15 IPMN cases, two distinct IPMN tumor samples were resected from patient MCC-PANC-PDO-017 located at the pancreatic head and body, respectively, for a total of 16 tumor samples. Thirteen of 16 IPMN tumor PDOs grew while 13 of 15 normal pancreatic organoids grew, for overall organoid generation success rates of 81% and 87%, respectively.

Cases with unsuccessful organoid development from IPMN tumor tissues were MCC-PANC-PDO-010, derived from an IPMN-pancreatobiliary subtype associated with invasive carcinoma; MCC-PANC-PDO-017, derived from an IPMN with high-grade dysplasia located at pancreatic body; and MCC-PANC-PDO-019, derived from an IPMN-pancreatobiliary subtype with high-grade dysplasia. Adjacent normal pancreatic tissues from MCC-PANC-PDO-017 and MCC-PANC-PDO-019 were also unsuccessful for organoid development.

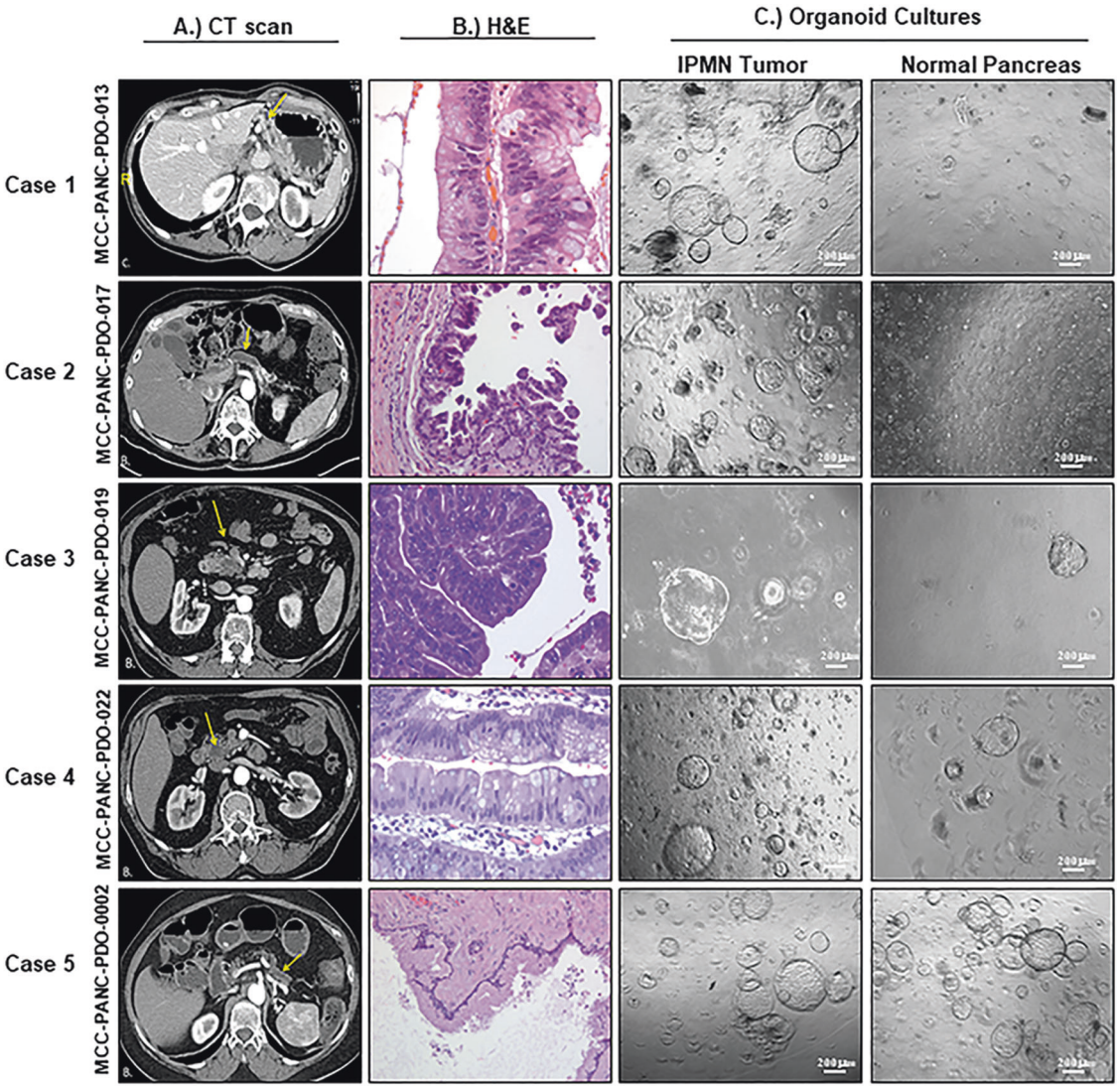

Fig. 2 Generation of organoids from characterized human resected IPMN and normal tissues. a Axial arterial phase preoperative computed tomography (CT) images of pancreatic IPMNs. **b** Hematoxylin and eosin (H&E) images of resected IPMN tumor tissue. **c** Bright-field micrographs (×5 magnification) of organoid cultures derived from resected IPMN tumors and adjacent normal pancreatic tissue around day 7 or 8 unless noted otherwise. *Case 1 (MCC-PANC-PDO-013)*: **a** Moderate pancreatic ductal dilatation is present in the pancreatic tail (arrow). **b** H&E (400X) shows high grade dysplasia of the mixed intestinal and gastric subtype characterized by pseudostratification with the nuclei remaining near the basal layer. The nuclei are vesicular with small nucleoli and visible goblet cells. *Case 2 (MCC-PANC-PDO-017)*: **a** Demonstrates diffuse irregular pancreatic main duct dilatation (arrows) compatible with main duct IPMN. **b** H&E (200X) shows columnar cells with basally located nuclei that merge into neoplastic cells with pseudostratification and high-grade architectural features. *Case 3 (MCC-PANC-PDO-019)*: **a** Shows a hypodense pancreatic head mass with subtle internal arterial phase enhancement (arrow). **b** H&E (400X) shows high grade dysplasia characterized by columnar neoplastic cells with eosinophilic cytoplasm. The nuclei overlap, are vesicular with nucleoli, and show loss of polarity and mitoses. **c** Organoids were isolated from frozen tissue 33 days post-resection for this high-grade IPMN of pancreatobiliary subtype. *Case 4 (MCC-PANC-PDO-022)*: **a** Hypodense mass (arrow) with mild internal enhancement in the pancreatic head. **b** H&E (400X) shows moderate grade dysplasia featuring papillary fronds lined by columnar, neoplastic cells, with pseudostratification and goblet cells. The nuclei are elongated and enlarged, with nuclear grooves. *Case 5 (MCC-PANC-PDO-0002)*: **a** Images through the pancreatic tail demonstrate diffuse dilatation of the main pancreatic duct (arrow). **b** High power showing basally located nuclei. This field shows low grade dysplasia of pancreatobiliary subtype. **c** Images taken at day 5. Scale bar, 200 mm.

Both normal pancreatic and IPMN organoids grew within 3 days. The majority of organoid cultures exhibited a cystic morphology (Fig. 2c). Tumor cultures with other morphologic features included MCC-PANC-PDO-013 and MCC-PANC-PDO-017, which exhibited a mixed morphology characterized by both cystic and solid-filled shapes (Fig. 2c). The organoid culture derived from frozen tissue, MCC-PANC-PDO-019, also exhibited a cystic morphology (Fig. 2c).

Table 1 Clinicopathological characteristics of the IPMN Study Cohort.

	Total ($n = 15$)	IPMN with low-grade dysplasia ($n = 3$)	IPMN with moderate-grade dysplasia ($n = 2$)	IPMN with high-grade dysplasia ($n = 7$)	Carcinoma arising from IPMN ($n = 3$)
Median age (years)	74	76	72	74	76
Gender (%)					
Male	9 (60)	2 (66.7)	1 (50)	3 (42.9)	3 (100)
Female	6 (40)	1 (33.3)	1 (50)	4 (57.1)	0
Clinical presentation (%)					
Symptomatic	9 (60)	2 (66.7)	1 (50)	4 (57.1)	2 (66.7)
Incidental finding	6 (40)	1 (33.3)	1 (50)	3 (42.9)	1 (33.3)
Location (%)					
Head	7 (43.8)	0	1 (50)	4 (50)	2 (66.7)
Uncinate process	3 (18.8)	1 (33.3)	1 (50)	1 (12.5)	0
Body	3 (18.8)	1 (33.3)	0	2 (25)	0
Tail	2 (12.5)	1 (33.3)	0	1 (12.5)	0
Diffuse	1 (6.2)	0	0	0	1 (33.3)
Biliary stent (%)					
Yes	1 (6.7)	0	0	0	1 (33.3)
No	14 (93.3)	3 (100)	2 (100)	7 (100)	2 (66.7)
Median CA 19-9 (U/mL)	18.1	18.2	42.3	15.1	24.3
Post-op tumor size (%)					
<3 cm	14 (87.5)	2 (66.7)	2 (100)	7 (87.5)	3 (100)
≥3 cm	2 (12.5)	1 (33.3)	0	1 (12.5)	0
Tumor stage (%)					
T_{is}	5 (31.3)	0	0	5 (62.5)	0
T1	2 (12.5)	0	1 (50)	0	1 (33.3)
T2	1 (6.2)	0	0	0	1 (33.3)
T3	1 (6.2)	0	0	0	1 (33.3)
Unspecified	7 (43.8)	3 (100)	1 (50)	3 (37.5)	0
Lymph node metastasis (%)					
No	9 (56.2)	0	1 (50)	5 (62.5)	3 (100)
Unspecified	7 (43.8)	3 (100)	1 (50)	3 (37.5)	0
Duct involvement					
Main duct	4 (25)	1 (33.3)	1 (50)	2 (25)	0
Branch ducts	1 (6.2)	0	0	1 (12.5)	0
Mixed	3 (18.8)	0	1 (50)	2 (25)	0
None	4 (25)	1 (33.3)	0	2 (25)	1 (33.3)
Unspecified	4 (25)	1 (33.3)	0	1 (12.5)	2 (66.7)
Subtype					
Pancreatobiliary	6 (37.5)	2 (66.7)	1 (50)	2 (25)	1 (33.3)
Intestinal	2 (12.5)	0	0	1 (12.5)	1 (33.3)
Foveolar/intestinal	1 (6.2)	0	0	1 (12.5)	0
Intestinal/pancreatobiliary	1 (6.2)	0	0	1 (12.5)	0
Intestinal/gastric	1 (6.2)	0	0	1 (12.5)	0
Gastric/pancreatobiliary	1 (6.2)	0	1 (50)	0	0
Unspecified	4 (25)	1 (33.3)	0	2 (25)	1 (33.3)

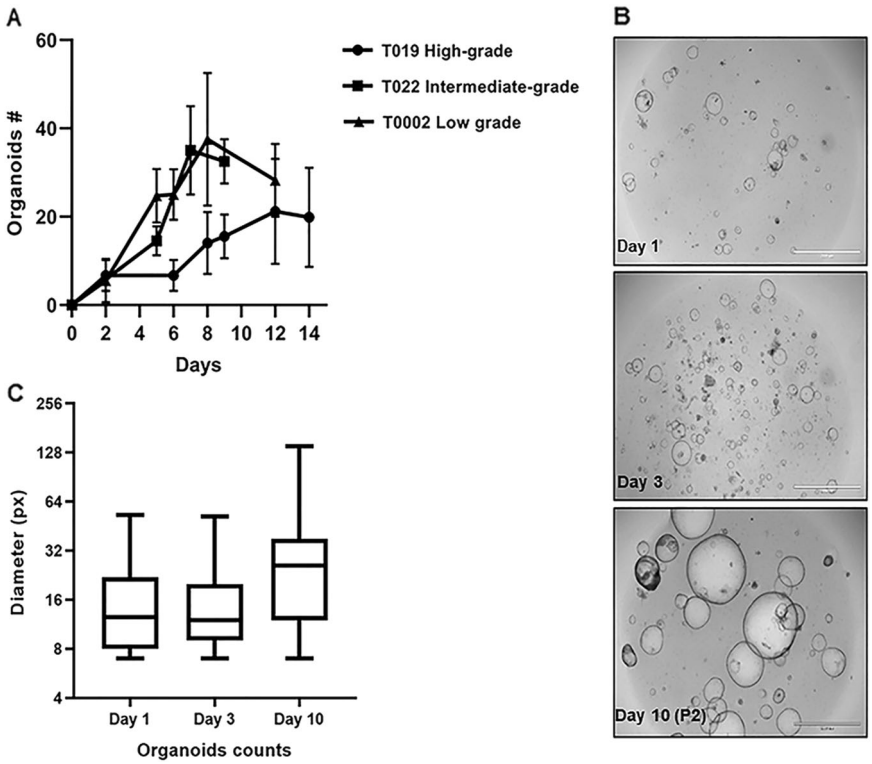

Fig. 3 Expansion and biobanking of cryopreserved human IPMN organoids. Growth rate of IPMN subtypes, passaging, and reviving. **a** Growth curve of patient-derived organoid culture from MCC-PANC-T019 high-grade IPMN of pancreatobiliary subtype, isolated from cryopreserved tissue 33 days post resection; MCC-PANC-T022 intermediate-grade IPMN of pancreatobiliary subtype isolated from fresh resected tissue; and MCC-PANC-T0002 low-grade IPMN of pancreatobiliary subtype from fresh resected tissue. **b** Patient-derived IPMN MCC-PANC-T005 organoid was revived 2 years post freezing, expanded, and passaged on Day 5 of culturing, then grown for an additional 10 days. Images were acquired on an EVOS FL Auto Imaging System, scale bar = 2 mm (×4 magnification). **c** MCC-PANC-T005 was analyzed by size (pxls) on the indicated days of culture.

We observed a different growth rate between the IPMN organoid cultures derived from fresh and frozen resected specimens. Organoids derived from fresh resected tissue grew at a faster rate than organoids derived from frozen resected tissue (Fig. 3a). In terms of grade of differentiation, organoid cultures derived from resected high-grade IPMNs grew at a slower rate than organoid cultures derived from low and intermediate/moderate-grade IPMN specimens (Fig. 3a).

Establishment and characterization of IPMN organoids

We successfully established 15 tumor IPMN PDO out of 20 samples using a modified version of an established procedure for tissue digestion [25]. This modified procedure uses wash media instead of feeding media for tissue digestion, making it a more cost-effective approach. These established IPMN PDO allowed long-term expansion and recovery after freezing. We were able to passage the IPMN PDO up to four times. Organoids from a second passage are shown in Fig. 3b. After two passages PDO-T005 size (pxls) were analyzed using the EVOS FL Auto Imaging System (Fig. 3c). We also successfully revived IPMN PDO that had been frozen for 2 years. Of note, we included Y-27632 Rho kinase inhibitor in the thawing media to help the organoid recover from the freeze/thaw stress; as others have described it as enhancing cells survival after cryopreservation [27, 28].

Morphological analysis of IPMN tumor organoids and primary tumors

Comparison of 3D brightfield images, H&E, and IHC stains for MUC5AC, CK19, and Ki-67 for four IPMN parental tumor samples and the derived organoids reveal that morphological structures of the parental tumor tissue are generally preserved in the organoids (Fig. 4a–d). For example, an H&E of the parental tissue for a low grade IPMN corresponds to an organoid that shows clusters with a central core surrounded by neoplastic cells (Fig. 4a) while parental tissue from a high grade IPMN reveals that the organoid grows in clusters (Fig. 4b). Expression levels of MUC5AC and CK19 are similar in the parental tumor and organoid for

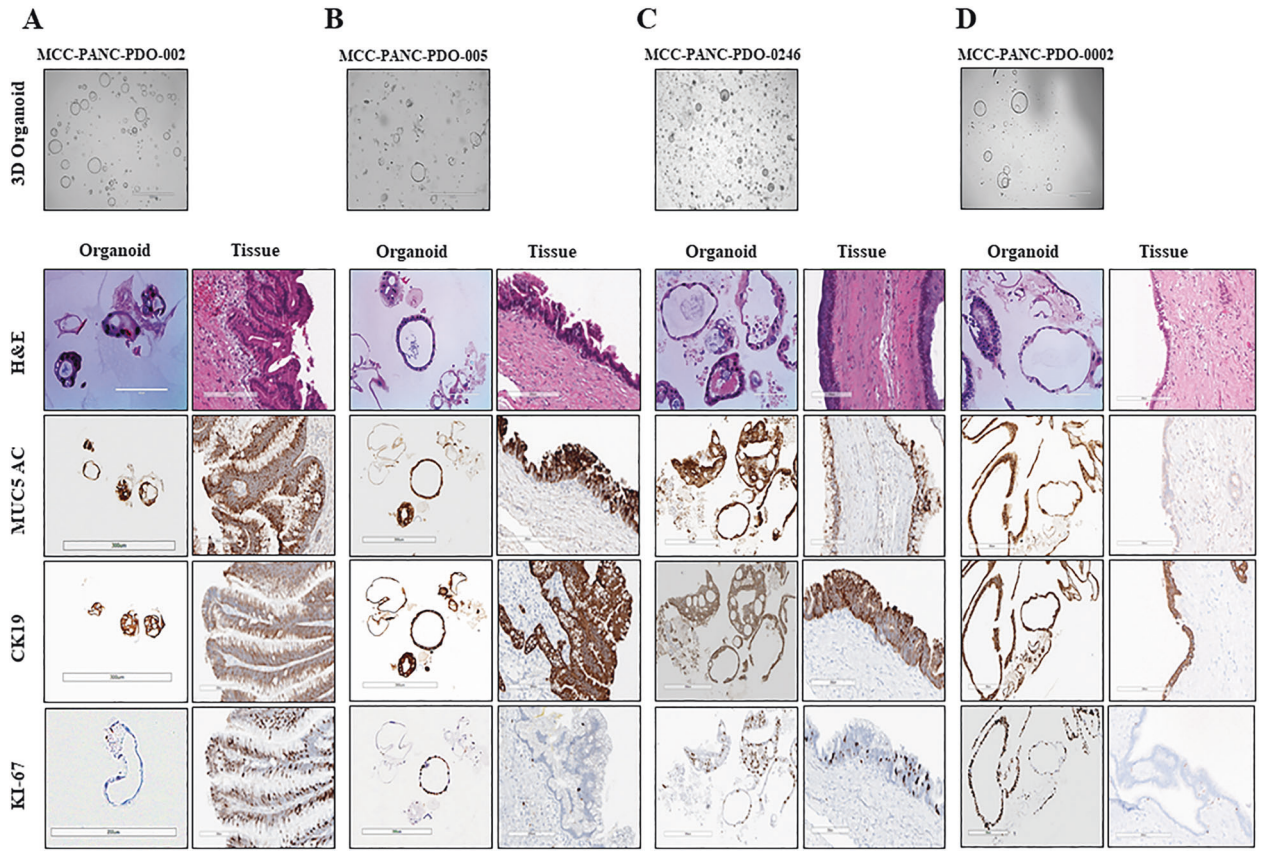

Fig. 4 Morphological analysis of IPMN tumor organoids and primary tumor. Morphological analysis of IPMN tumor organoids and primary tumors. Shown are 3D Brightfield images and H&E and immunohistochemical studies for MUC5AC, CK19, and Ki-67 for four IPMN tumor tissue samples and their derived organoids. **a** MCC-PANC-PDO-002. The H&E of the tissue shows a low grade IPMN. The organoid shows clusters with a central core surrounded by neoplastic cells. Both the organoid and tissue strongly express MUC5AC, CK19. The tissue has a higher Ki-67 proliferation index than the organoid. **b** MCC-PANC-PDO-005. Tissue is a high grade IPMN. The organoid grows in clusters. The MUC5AC and CK 19 show a comparable expression level. The organoid cluster shows a higher Ki-67 than the tissue in this field. **c** MCC-PANC-PDO-0246. The tissue shows low-grade IPMN. The MUC5AC, CK19, and ki-67 expression levels are similar in the organoid and tissue. **d** MCC-PANC-PDO-0002. The tissue shows low grade IPMN with attenuated lining epithelium secondary to previous fine needle aspiration of the cyst. The CK19 expression levels are similar. The MUC5AC shows faint cytoplasmic expressions, but the expression in the organoid is strong. The organoid and tissue show similar expression for CK19. The Ki-67 is higher in the organoid sample.

several cases (Fig. 4a–c) and remains independent of whether organoids were freshly generated, PDO-0246 (Fig. 4c) or revived, PDO-002, PDO-005, and PDO-0002 (Fig. 4d). The expression levels of Ki-67 staining are similar in both organoids and its parental tissue (Fig. 4b–d).

Organoid imaging and automated counting

Images of the organoids were captured with a bright-field microscope at a magnification low enough to include the whole sample. The images were processed and analyzed via Image-Pro Premier software. Quantification of organoids can be challenging because they are grown in a 3D culture environment. Overlapping of the organoids makes it difficult for the available automated segmentation technique to give an accurate count. In order to develop a protocol for counting organoids in vitro, the Moffitt Imaging Response Assessment Team Core optimized the CHT based algorithm [29] to detect overlapping circular objects. We successfully quantitated organoids and segmented them by size (pxls) using this technique (Fig. 5a–c).

Genomic characterization of IPMN organoids

DNA was isolated from both normal and IPMN tumor organoids that showed successful growth, and was successfully performed on fresh and cryopreserved organoid samples. The concentration of DNA from normal samples ranged from 2.72 to 10 ng/μL and total DNA ranged from 44 to 223 ng. Their DIN scores ranged from 3.4 to 8. The concentration of DNA from IPMN tumor samples ranged from 2.32 to 33.2 ng/μL, the total DNA yields ranged from 131 to 672 ng, and the DIN scores ranged from 2.9 to 7.8.

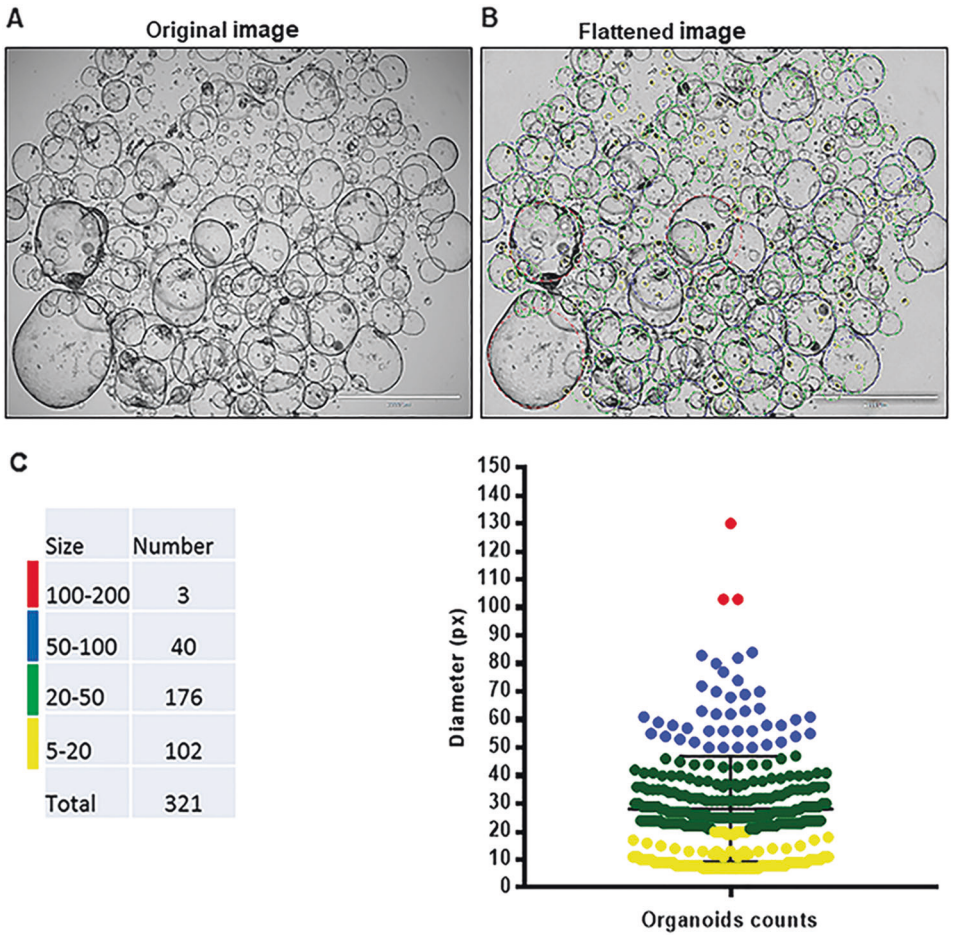

Fig. 5 Automated counting of organoids using a Circular Hough Transform (CHT) based algorithm. Patient-derived organoid culture of low-grade IPMN of pancreatobiliary subtype (MCC-PANC-T0002) was revived, expanded, and passage twice. Image acquired at day 6 post passage. **a** Original image acquired on an EVOS FL Auto Imaging System (×1.25 objective). **b** Flattened image and segmentation of detected objects. Scale bar = 2 mm. **c** Distribution of organoids based on count and size. Resulting organoid count color was coded by size (pxls).

All samples that underwent DNA fingerprinting passed quality control criteria and had single nucleotide polymorphism (SNP) genotype call rates that approached 100%. In addition, the same identity for each PDO tumor-normal pair was verified, with nearly perfect correlations ($r^2 > 0.99$) observed when comparing the allele intensity of samples in each pair. As expected, tumor and normal samples from unrelated individuals did not show correlated genotypes ($r^2 < 0.10$).

In order to further characterize the IPMN organoids and determine whether their genomic profile matched their tissue of origin, four pairs of organoids and their corresponding paired parental tumor and normal tissue underwent targeted sequencing of cancer-associated genes using the QIAseq Human Comprehensive Cancel Panel. Average read depth of coverage ranged from 356× to 1201×, and average molecular barcode read depth of coverage was 20× to 170×. We observed an average of 41.5 somatic mutations in the targeted sequencing of organoids derived from IPMN tumors. Recurrent protein-altering somatic mutations were identified in key genes including *KRAS, GNAS, RNF43*, and *BRAF*, with somatic mutations identified in 2 (50%), 1 (25%), 1 (25%), and 1 (25%) of the four IPMN PDOs, respectively (Fig. 6). Importantly, somatic mutations identified in the organoids were often found in the corresponding tumors (although tumor heterogeneity was observed), highlighting the potential for organoids to recapitulate genetic alterations commonly found in a premalignant disease state [30, 31]. For example, KRAS G12D and GNAS R844C were found in both the PDO and parental tumor for case 022, while *KRAS* mutations (G12D and G12V) observed in the PDO for case 0264 had evidence in the parental IPMN tumor, but at a lower frequency. For cases that did not have shared mutations between the parental tumor and PDO, it is possible that a different subclone was sequenced from the parent tumor tissue during the organoid culture process. An oncoprint showcasing protein-altering mutations in additional genes found in the PDO and parental tumors is featured in Supplementary Fig. S1.

Discussion

We report the feasibility of generating viable patient-derived IPMN tumor and normal pancreatic organoids

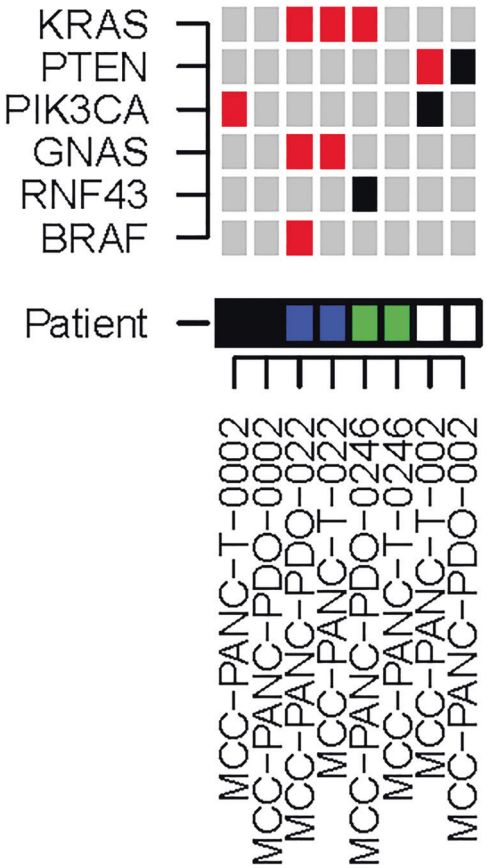

Fig. 6 Characterization of IPMN tumor organoids by DNA sequencing. Oncoprint demonstrates that genes known to be mutated in IPMN tumors (*KRAS, PTEN, PIK3CA, GNAS, RNF43*, and *BRAF)* are mutated in a subset of paired IPMN parental tumor (T) and PDO samples from pathologically-confirmed low-grade (T002, T0002, T0246), and moderate-grade (T022) IPMN cases. Red boxes indicate protein-altering mutations, and black boxes indicate protein-truncating mutations.

from newly resected and cryopreserved tissue at a success rate of 81% and 87%, respectively. Our outcomes are similar to previously-reported success rates of human pancreatic organoid models derived from normal and pancreatic ductal adenocarcinoma, which were up to 80% and 87%, respectively [18, 22, 32–34]. The IPMN organoids were passaged, cryopreserved, and imaged with digital platforms [29, 35, 36], which proved to be suitable to determine the number of overlapping organoids and organoid size over time. The IPMN PDO we generated exhibited a range of morphologies characterized by cystic and solid-filled spheres as previously described in organoid models derived from primary pancreatic cells and tissues [34, 37, 38]. Finally, histologic and genomic characterization of a subset of IPMN organoids and the paired parental tumor was successfully performed.

The establishment and expansion of pancreatic organoid cultures can require a 2-week to 5-month timeframe [34, 37, 38], taking less time depending on the quantity of resected tissue available [39]. For example, over a 90% success rate has been reported for generation of colorectal cancer organoids with adequate amount of specimen [20]. In this investigation, IPMN organoid cultures were optimally established by a 2-week incubation followed by passage and cryopreservation. Growth rate differences were observed between low-grade and high-grade IPMNs, with high-grade IPMNs growing at a slower pace than low-grade IPMNs. Although this may be linked to distinct genetic and stromal factors that may impede growth and may be specific to individual patients [39], this observation was based on a small number of samples and warrants replication before drawing any firm conclusions.

We showed that the organoid culture model can recapitulate the morphological and mutational profiles of resected IPMNs, consistent with existing data on primary PDAC tumors [18–21] and a recently published manuscript on IPMNs [23]. Discordance of somatic mutations was reported in several parental tumor-PDO pairs, suggesting a different subclone of parental tissue may have been sequenced compared to the subclone(s) that grew into organoid culture, consistent with prior studies which reveal driver gene heterogeneity in IPMNs [23, 40].

There are several areas that need to be addressed before translational advances can be made. For example, it is important to assess factors that may have resulted in organoid isolation failure (including tissue growth requirements [41] and slight deviations of protocols that may have impacted tissue processing after acquisition, tissue quality, and digestion time) [31]. Also, the Wnt ligands often do not possess sufficient activity to promote organoid growth; therefore, its monitoring is recommended to ensure optimal culture conditions [42]. The establishment of normal and tumor organoids under the same conditions may favor overgrowth of normal epithelial cells and halt organoid isolation [43]. High levels of genomic instability may lead to organoid apoptosis which may have posed a challenge upon generation and passage of organoid cultures [43]. Other biological factors such as sampling variation from heterogeneous tumors, evolution, natural selection due to culture conditions, stromal components, and tumor necrosis may have contributed to the characteristic mutational profile of the organoids [44]. Finally, despite advances in 3D culture techniques, long-term expansion remains a challenge [22]. Difficulties reviving the organoids were encountered and lengthy optimization techniques were performed in order to revive and expand the IPMN organoids, making survival beyond four passages a challenge as organoids did not maintain their structure and viability. Of note, Huang et al. [23] also reported survival for up to four passages in their new IPMN organoid

living biobank. There is a possibility that IPMN PDO require additional manipulation of the culture condition that would favor their expansion using newly described modifications [31].

Despite these challenges, the organoid platform may foster an improved understanding of the histopathology, genetic mechanisms, and stromal interactions of pancreatic cancer precursors and provide insight into novel chemoprevention and treatment approaches [45]. There is also potential to generate organoids from pancreatic biopsy specimens [46–48] since fine needle biopsies can be a sufficient source of cells to isolate organoids within two weeks, with a success rate of 87% [33, 44]. The capacity to generate these preclinical models from surgical specimens and biopsies also has great potential to foster personalized medicine approaches to combine the high-throughput drug screening with the molecular assessment of organoid models in order to identify key diagnostic and therapeutic biomarkers that will predict which patients are at a higher risk of progression [49]. Furthermore, based on studies that have shown the ability of CRISPR/Cas9-mediated genome editing to modify driver genes in human pancreatic ductal organoids, opportunity exists to replicate the genetic mechanisms leading to pancreatic tumorigenesis [50–52].

In summary, this is the largest reported IPMN PDO living biobank derived from human resected tissues that we are aware of. The generation, passage, cryopreservation, and characterization of these models demonstrate feasibility in this approach, which may ultimately enable clinical implementation in favor of improving patient outcomes and chemoprevention studies aimed to halt progression of IPMN to invasive cancer.

Acknowledgements The research supported in this publication was supported in part by a Moffitt Cancer Center Team Science Award (awarded to JPB, DJ, GMD, MM, KJ, and D-TC), the James and Esther King Biomedical Research Program, Florida Department of Health (Grant #8JK02; awarded to JPB), and the Tissue Core, Molecular Genomics Core, Analytic Microscopy Core, the Imaging Response Assessment Team, and the Biostatistics and Bioinformatics Shared Resource at the H. Lee Moffitt Cancer Center & Research Institute, an NCI designated Comprehensive Cancer Center (P30-CA076292). The content is solely the responsibility of the authors and does not necessarily represent the official views of the sponsors or the H. Lee Moffitt Cancer Center & Research Institute. Editorial assistance was provided by the Moffitt Cancer Center's Scientific Editing Department by Dr. Paul Fletcher & Daley Drucker. No compensation was given beyond their regular salaries. The authors also wish to thank Warren Gloria, Karen Coley, Rithi Somesh Shivaram, Dennis Hall, and Vyacheslav Petrovskyy for their assistance with pathological review of tissues in the gross room.

Compliance with ethical standards

Conflict of interest There are no conflicts of interest.

References

1. Bray F, Ferlay J, Soerjomataram I, Siegel RL, Torre LA, Jemal A. Global cancer statistics 2018: GLOBOCAN estimates of incidence and mortality worldwide for 36 cancers in 185 countries. CA Cancer J Clin. 2018;68:394–424.
2. Ferlay J, Ervik M, Lam F, Colombet M, Mery L, Piñeros M, et al. Global Cancer Observatory: Caner Today. Lyon, France: International Agency for Research on Cancer; 2018. Accessed 21 Feb 2019.
3. American Cancer Society. Cancer Facts & Figures. 2020.
4. Rawla P, Sunkara T, Gaduputi V. Epidemiology of pancreatic cancer: global trends, etiology and risk factors. World J Oncol. 2019;10:10–27.
5. Saad AM, Turk T, Al-Husseini MJ, Abdel-Rahman O. Trends in pancreatic adenocarcinoma incidence and mortality in the United States in the last four decades; a SEER-based study. BMC Cancer. 2018;18:688.
6. Patel N, Khorolsky C, Benipal B. Incidence of pancreatic adenocarcinoma in the United States from 2001 to 2015: A United States cancer statistics analysis of 50 states. Cureus. 2018;10:e3796.
7. Gordon-Dse agu VL, Devesa SS, Goggins M, Stolzenberg-Solomon R. Pancreatic cancer incidence trends: evidence from the Surveillance, Epidemiology and End Results (SEER) population-based data. Int J Epidemiol. 2018;47:427–39.
8. Wong MCS, Jiang JY, Liang M, Fang Y, Yeung MS, Sung JJY. Global temporal patterns of pancreatic cancer and association with socioeconomic development. Sci Rep. 2017;7:3165.
9. Rahib L, Smith BD, Aizenberg R, Rosenzweig AB, Fleshman JM, Matrisian LM. Projecting cancer incidence and deaths to 2030: the unexpected burden of thyroid, liver, and pancreas cancers in the United States. Cancer Res. 2014;74:2913–21.
10. Farrell JJ. Prevalence, diagnosis and management of pancreatic cystic neoplasms: current status and future directions. Gut Liver. 2015;9:571–89.
11. Basar O, Brugge WR. My treatment approach: pancreatic cysts. Mayo Clin Proc. 2017;92:1519–31.
12. Furukawa T, Kloppel G, Volkan Adsay N, Albores-Saavedra J, Fukushima N, Horii A, et al. Classification of types of intraductal papillary-mucinous neoplasm of the pancreas: a consensus study. Virchows Arch. 2005;447:794–9.
13. Kang MJ, Lee KB, Jang JY, Han IW, Kim SW. Evaluation of clinical meaning of histological subtypes of intraductal papillary mucinous neoplasm of the pancreas. Pancreas. 2013;42:959–66.
14. Hackert T, Fritz S, Klauss M, Bergmann F, Hinz U, Strobel O, et al. Main-duct intraductal papillary mucinous neoplasm: high cancer risk in duct diameter of 5 to 9 mm. Ann Surg. 2015;262:875–80. Discussion 80–1.
15. Lafemina J, Katabi N, Klimstra D, Correa-Gallego C, Gaujoux S, Kingham TP, et al. Malignant progression in IPMN: a cohort analysis of patients initially selected for resection or observation. Ann Surg Oncol. 2013;20:440–7.
16. Elta GH, Enestvedt BK, Sauer BG, Lennon AM. ACG clinical guideline: diagnosis and management of pancreatic cysts. Am J Gastroenterol. 2018;113:464–79.
17. Choi SH, Park SH, Kim KW, Lee JY, Lee SS. Progression of unresected intraductal papillary mucinous neoplasms of the pancreas to cancer: a systematic review and meta-analysis. Clin Gastroenterol Hepatol. 2017;15:1509–20.e4.
18. Tiriac H, Belleau P, Engle DD, Plenker D, Deschenes A, Somerville TDD, et al. Organoid profiling identifies common

responders to chemotherapy in pancreatic cancer. Cancer Discov. 2018;8:1112–29.
19. Romero-Calvo I, Weber CR, Ray M, Brown M, Kirby K, Nandi RK, et al. Human organoids share structural and genetic features with primary pancreatic adenocarcinoma tumors. Mol Cancer Res. 2019;17:70–83.
20. van de Wetering M, Francies HE, Francis JM, Bounova G, Iorio F, Pronk A, et al. Prospective derivation of a living organoid biobank of colorectal cancer patients. Cell. 2015;161:933–45.
21. Gendoo DMA, Denroche RE, Zhang A, Radulovich N, Jang GH, Lemire M, et al. Whole genomes define concordance of matched primary, xenograft, and organoid models of pancreas cancer. PLoS Comput Biol. 2019;15:e1006596.
22. Boj SF, Hwang CI, Baker LA, Chio II, Engle DD, Corbo V, et al. Organoid models of human and mouse ductal pancreatic cancer. Cell. 2015;160:324–38.
23. Huang B, Trujillo MA, Fujikura K, Qiu M, Chen F, Felsenstein M, et al. Molecular characterization of organoids derived from pancreatic intraductal papillary mucinous neoplasms. J Pathol. 2020. https://doi.org/10.1002/path.5515. [Epub ahead of print].
24. Permuth JB, Trevino J, Merchant N, Malafa M. Partnering to advance early detection and prevention efforts for pancreatic cancer: the Florida Pancreas Collaborative. Future Oncol. 2016;12:997–1000.
25. Baker L, Tiriac H, Corbo V, Young CM. Tuveson laboratory murine and human organoid protocols. Cold Spring Harbor Laboratory. 2017.
26. Huch M, Bonfanti P, Boj SF, Sato T, Loomans CJ, van de Wetering M, et al. Unlimited in vitro expansion of adult bi-potent pancreas progenitors through the Lgr5/R-spondin axis. Embo J. 2013;32:2708–21.
27. Clinton J, McWilliams-Koeppen P. Initiation, expansion, and cryopreservation of human primary tissue-derived normal and diseased organoids in embedded three-dimensional culture. Curr Protoc Cell Biol. 2019;82:e66.
28. Li X, Meng G, Krawetz R, Liu S, Rancourt DE. The ROCK inhibitor Y-27632 enhances the survival rate of human embryonic stem cells following cryopreservation. Stem Cells Dev. 2008;17:1079–85.
29. Atherton TJ, Kerbyson DJ. Size invariant circle detection. Image and Vision Comput. 1999;17:795–803.
30. Driehuis E, van Hoeck A, Moore K, Kolders S, Francies HE, Gulersonmez MC, et al. Pancreatic cancer organoids recapitulate disease and allow personalized drug screening. Proc Natl Acad Sci USA. 2019;116:26580–90.
31. Georgakopoulos N, Prior N, Angres B, Mastrogiovanni G, Cagan A, Harrison D, et al. Long-term expansion, genomic stability and in vivo safety of adult human pancreas organoids. BMC Dev Biol. 2020;20:4.
32. Huang L, Holtzinger A, Jagan I, BeGora M, Lohse I, Ngai N, et al. Ductal pancreatic cancer modeling and drug screening using human pluripotent stem cell- and patient-derived tumor organoids. Nat Med. 2015;21:1364–71.
33. Tiriac H, Bucobo JC, Tzimas D, Grewel S, Lacomb JF, Rowehl LM, et al. Successful creation of pancreatic cancer organoids by means of EUS-guided fine-needle biopsy sampling for personalized cancer treatment. Gastrointest Endosc. 2018;87:1474–80.
34. Baker LA, Tiriac H, Tuveson DA. Generation and culture of human pancreatic ductal adenocarcinoma organoids from resected tumor specimens. In: Pancreatic Cancer. Clifton, N.J.: Springer; 2019. p. 97–115.
35. Yuen H, Princen J, Illingworth J, Kittler J. Comparative study of Hough transform methods for circle finding. Image Vision Comput. 1990;8:71–7.
36. Davies ER. Machine vision: theory, algorithms, practicalities. Elsevier; 2004.
37. Baker LA, Tiriac H, Clevers H, Tuveson DA. Modeling pancreatic cancer with organoids. Trends Cancer. 2016;2:176–90.
38. Hou S, Tiriac H, Sridharan BP, Scampavia L, Madoux F, Seldin J, et al. Advanced development of primary pancreatic organoid tumor models for high-throughput phenotypic drug screening. SLAS Discov. 2018;23:574–84.
39. Aberle MR, Burkhart RA, Tiriac H, Olde Damink SWM, Dejong CHC, Tuveson DA, et al. Patient-derived organoid models help define personalized management of gastrointestinal cancer. Br J Surg. 2018;105:e48–60.
40. Fischer CG, Beleva Guthrie V, Braxton AM, Zheng L, Wang P, Song Q, et al. Intraductal papillary mucinous neoplasms arise from multiple independent clones, each with distinct mutations. Gastroenterology. 2019;157:1123–37.e22.
41. Miyoshi H, Stappenbeck TS. In vitro expansion and genetic modification of gastrointestinal stem cells in spheroid culture. Nat Protoc. 2013;8:2471–82.
42. Tuysuz N, van Bloois L, van den Brink S, Begthel H, Verstegen MM, Cruz LJ, et al. Lipid-mediated Wnt protein stabilization enables serum-free culture of human organ stem cells. Nat Commun. 2017;8:14578.
43. Karthaus WR, Iaquinta PJ, Drost J, Gracanin A, van Boxtel R, Wongvipat J, et al. Identification of multipotent luminal progenitor cells in human prostate organoid cultures. Cell. 2014;159:163–75.
44. Weeber F, van de Wetering M, Hoogstraat M, Dijkstra KK, Krijgsman O, Kuilman T, et al. Preserved genetic diversity in organoids cultured from biopsies of human colorectal cancer metastases. Proc Natl Acad Sci USA. 2015;112:13308–11.
45. Miller MS, Allen P, Brentnall TA, Goggins M, Hruban RH, Petersen GM, et al. Pancreatic cancer chemoprevention translational workshop: meeting report. Pancreas. 2016;45:1080–91.
46. Khorana AA, Mangu PB, Berlin J, Engebretson A, Hong TS, Maitra A, et al. Potentially curable pancreatic cancer: american society of clinical oncology clinical practice guideline update. J Clin Oncol. 2017;35:2324–8.
47. Winter JM, Cameron JL, Campbell KA, Arnold MA, Chang DC, Coleman J, et al. 1423 pancreaticoduodenectomies for pancreatic cancer: a single-institution experience. J Gastrointest Surg. 2006;10:1199–210. Discussion 210–1.
48. Tiriac H, Plenker D, Baker LA, Tuveson DA. Organoid models for translational pancreatic cancer research. Curr Opin Genet Dev. 2019;54:7–11.
49. Pauli C, Hopkins BD, Prandi D, Shaw R, Fedrizzi T, Sboner A, et al. Personalized in vitro and in vivo cancer models to guide precision medicine. Cancer Discov. 2017;7:462–77.
50. Fujii M, Clevers H, Sato T. Modeling human digestive diseases with CRISPR-Cas9-modified organoids. Gastroenterology. 2019;156:562–76.
51. Seino T, Kawasaki S, Shimokawa M, Tamagawa H, Toshimitsu K, Fujii M, et al. Human pancreatic tumor organoids reveal loss of stem cell niche factor dependence during disease progression. Cell Stem Cell. 2018;22:454–67.e6.
52. Lee J, Snyder ER, Liu Y, Gu X, Wang J, Flowers BM, et al. Reconstituting development of pancreatic intraepithelial neoplasia from primary human pancreas duct cells. Nat Commun. 2017;8:14686.

Affiliations

Francisca Beato[1] · Dayana Reverón[2] · Kaleena B. Dezsi[3] · Antonio Ortiz[4] · Joseph O. Johnson[4] · Dung-Tsa Chen[5] · Karla Ali[3] · Sean J. Yoder[6] · Daniel Jeong[7] · Mokenge Malafa[1] · Pamela Hodul[1] · Kun Jiang[8] · Barbara A. Centeno[8] · Mahmoud A. Abdalah[9] · Jodi A. Balasi[10] · Alexandra F. Tassielli[1] · Bhaswati Sarcar[1] · Jamie K. Teer[5] · Gina M. DeNicola[11] · Jennifer B. Permuth[1,3] · Jason B. Fleming[1]

[1] Department of Gastrointestinal Oncology, Moffitt Cancer Center and Research Institute, Tampa, FL, USA

[2] Ponce Health Sciences University, Ponce, PR, USA

[3] Department of Cancer Epidemiology, Moffitt Cancer Center and Research Institute, Tampa, FL, USA

[4] Analytical Microscopy Core Facility, Moffitt Cancer Center and Research Institute, Tampa, FL, USA

[5] Department of Biostatistics and Bioinformatics, Moffitt Cancer Center and Research Institute, Tampa, FL, USA

[6] Molecular Genomics Core Facility, Moffitt Cancer Center and Research Institute, Tampa, FL, USA

[7] Department of Diagnostic Imaging, Moffitt Cancer Center and Research Institute, Tampa, FL, USA

[8] Department of Anatomic Pathology, H. Lee Moffitt Cancer Center and Research Institute, Tampa, FL, USA

[9] Imaging Response Assessment Team Core Facility, H. Lee Moffitt Cancer Center and Research Institute, Tampa, FL, USA

[10] Tissue Core Histology, H. Lee Moffitt Cancer Center and Research Institute, Tampa, FL, USA

[11] Department of Cancer Physiology, Moffitt Cancer Center and Research Institute, Tampa, FL, USA